



RESEARCH ARTICLE

IFN γ protects motor neurons from oxidative stress via enhanced global protein synthesis in FUS-associated amyotrophic lateral sclerosis

Amanda Faria Assoni^{1,2} | Erika N. Guerrero^{1,3} | René Wardenaar¹ |
 Danyllo Oliveira² | Petra L. Bakker¹ | Luciana M. Alves² |
 Valdemir M. Carvalho⁴  | Oswaldo Keith Okamoto² | Mayana Zatz² |
 Floris Fojer¹ 

¹European Research Institute for the Biology of Ageing (ERIBA), University of Groningen, University Medical Center Groningen, Groningen, The Netherlands

²Instituto de Biociências, Universidade de São Paulo, São Paulo, Brazil

³Department of Stem Cell Research, Gorgas Memorial Institute for Health Studies, Panama City, Republic of Panama

⁴Division of Research and Development, Fleury Group, São Paulo, Brazil

Correspondence

Floris Fojer, European Research Institute for the Biology of Ageing (ERIBA), University of Groningen, University Medical Center Groningen, Groningen, 9713 AV, The Netherlands.

Email: f.fojer@umcg.nl

Abstract

Amyotrophic lateral sclerosis type 6 (ALS6) is a familial subtype of ALS linked to Fused in Sarcoma (FUS) gene mutation. FUS mutations lead to decreased global protein synthesis, but the mechanism that drives this has not been established. Here, we used ALS6 patient-derived induced pluripotent stem cells (hiPSCs) to study the effect of the ALS6 FUS^{R521H} mutation on the translation machinery in motor neurons (MNs). We find, in agreement with findings of others, that protein synthesis is decreased in FUS^{R521H} MNs. Furthermore, FUS^{R521H} MNs are more sensitive to oxidative stress and display reduced expression of TGF- β and mTORC gene pathways when stressed. Finally, we show that IFN γ treatment reduces apoptosis of FUS^{R521H} MNs exposed to oxidative stress and partially restores the translation rates in FUS^{R521H} MNs. Overall, these findings suggest that a functional IFN γ response is important for FUS-mediated protein synthesis, possibly by FUS nuclear translocation in ALS6.

1 | INTRODUCTION

Amyotrophic lateral sclerosis (ALS) is a late-onset neurodegenerative disease that affects motor neurons (MNs) in the motor cortex, brainstem, and spinal cord [1]. It is characterized by muscle twitching, spasms, stiffness, weakness, and finally, muscle atrophy with a life expectancy of 3–5 years after diagnosis [2]. ALS is the most common MN disease with an average prevalence and incidence of 4.42 and 1.59 per 1,000,000 population which increases with age [3]. In ~90% of the cases, ALS is sporadic, but ~10% of patients show familial mutations (Mathis et al., 2019). ALS subtypes are classified according to the affected gene, which includes Superoxide Dismutase 1 (SOD1; ALS1), TAR DNA

Binding Protein-43 (TDP-43; ALS10), Chromosome 9 Open Reading Frame (C9ORF72; ALS1) and Fused in Sarcoma (FUS; ALS6) [4], the latter leading to one of the most aggressive and early onset types of ALS [5].

FUS is a component of the heterogeneous nuclear ribonucleoprotein protein complex (hnRNP) and a DNA/RNA-binding protein involved in DNA damage repair, splicing, and multiple aspects of RNA metabolism [6, 7]. More than 50 different mutations in the FUS gene have so far been identified in ALS6 patients [8]. While some mutations affect the N-terminal region, arginine-glycine-glycine box (RGG) and RNA recognition motif (RRM) region, most missense mutations affect the nuclear localization signal (NLS) domain in the C-terminus of the protein. These mutations result in

This is an open access article under the terms of the [Creative Commons Attribution-NonCommercial-NoDerivs](https://creativecommons.org/licenses/by-nc-nd/4.0/) License, which permits use and distribution in any medium, provided the original work is properly cited, the use is non-commercial and no modifications or adaptations are made.

© 2023 The Authors. *Brain Pathology* published by John Wiley & Sons Ltd on behalf of International Society of Neuropathology.

cytoplasmic mislocalization and nuclear clearance of FUS and yield an aggressive disease phenotype [9, 10]. The most common FUS mutation affects arginine 521 (R to H, C, or G) [11]. FUS mislocalization is not unique to ALS6 but also occurs in other familial forms of ALS and sporadic cases where FUS itself is not mutated [12]. However, how FUS mutations lead to MN death in ALS remains unclear.

Strategies to study the pathobiology of ALS are challenging since biopsies are associated with high cost and morbidity and do not provide a definitive pathological diagnosis [13]. Therefore, reliable models of the disease are key to elucidating the molecular mechanisms underlying ALS. In this study, we use iPSCs derived from ALS6 patients carrying a FUS^{R521H} mutation to generate MNs to study ALS disease biology. As iPSCs rejuvenate as a result of reprogramming [14] and ALS symptoms present with ageing, we expose iPSC-derived motor neurons to oxidative stress to model ageing-associated effects [15]. Although patient-derived iPSCs present limitations in their ability to simulate age-associated traits, we consider this model crucial for understanding early phenotypes that could lead to the development of therapeutics that may prevent disease progression. Our models reveal that MNs generated from ALS6 patient-derived iPSCs show aberrant cytoplasmic localization of FUS and decreased translation rates. Furthermore, FUS^{R521H} iPSC-derived MNs are more susceptible to oxidative stress-induced apoptosis than MNs differentiated from iPSCs generated from unaffected family members. This increased susceptibility coincides with decreased TGF- β and mTOR signaling and an altered cytokine landscape. Intriguingly, we find that supplementation of IFN γ to FUS^{R521H} MN-cultures reduces oxidative stress-induced apoptosis significantly, which coincides with improved translation rates and nuclear FUS localization. Overall, our results show that IFN γ treatment reduces sensitivity to oxidative stress specifically of FUS^{R521H} MNs. While further work is required to understand how IFN γ restores FUS localization and impaired translation rates, our findings suggest that early-diagnosed ALS6 patients might benefit from IFN γ treatment to slow down disease progression.

2 | RESULTS

2.1 | iPSC-derived MNs from ALS6 patients are susceptible to oxidative stress-induced apoptosis

To investigate how mutant FUS affects the biology of MNs, we generated iPSC lines from 2 ALS6 patients carrying the FUS^{R521H} mutation alongside with 2 iPSC lines from phenotypically healthy relatives not carrying the mutation (from now on referred to as “control”). iPSCs were differentiated into mature MNs according to an established protocol [16] (Figure 1A) followed by immunofluorescence (IF) stainings

for HB9, MAP2, and MN-specific markers Tuj1, Islet1 to confirm complete differentiation (Figure 1B). We then compared cell viability and apoptosis rates between control and FUS^{R521H} iPSCs, neural progenitor cells, and mature MNs, but found no significant differences (Figure 1C, D). As oxidative stress has been proposed as a driving factor in ALS [17], cells were treated with sodium arsenite (SA), a well-known inducer of oxidative stress through the generation of reactive oxygen species (ROS) [18]. FUS^{R521H} mature MNs were significantly more sensitive to SA treatment compared to healthy controls, evidenced by lower viability (Figures 1E, F, S1D; data presented for individual experiments); Figure S1E (data for additional iPSC lines) and increased apoptosis following treatment (Figure 1G, H, S1F; data presented for individual experiments); Figure S1G (data for additional iPSC lines). We conclude that FUS^{R521H} and control iPSCs, NPCs, and MNs have similar viability under unperturbed conditions, but that FUS^{R521H}-derived MNs are more sensitive to oxidative stress induced by SA.

2.2 | FUS^{R521H} motor neurons show altered expression of genes in the mTOR pathway and genes related to the innate immune response system

To explore why FUS^{R521H} MNs are more sensitive to oxidative stress than controls, we compared the transcriptomes of FUS^{R521H} and control MNs, either or not treated with SA, by RNA sequencing. Interestingly, FUS^{R521H} MNs showed increased innate immune system (i.e., “complement”) transcripts compared to healthy control MNs (Figure 1I), but only when not treated with SA. In contrast, SA-treated FUS^{R521H} MNs showed decreased expression of genes involved in TGF- β and mTORC signaling compared to SA-treated healthy controls (Figure 1J). As TGF- β is critical for the activation of cytokines [19, 20], next we measured cytokines secreted by FUS^{R521H} MNs when exposed to oxidative stress using a cytokine multiplex assay. Indeed, we found that ALS6 MNs secrete more IL-8 and CCL2, and less IFN γ and IL-15 when treated with SA (Figure 1K). In line with this, we also found that control MNs upregulate IFN γ signaling following SA treatment (Figure S1A), but ALS MNs fail to do so (Figure S1B). These observations suggest that FUS^{R521H} MNs show an impaired response to oxidative stress involving decreased TGF- β and mTORC signaling and an altered cytokine landscape including reduced IFN γ .

2.3 | Global translation rates are decreased in FUS^{R521H} NPs and MNs

As FUS^{R521H} MNs displayed reduced expression of genes involved in mTORC signaling following SA

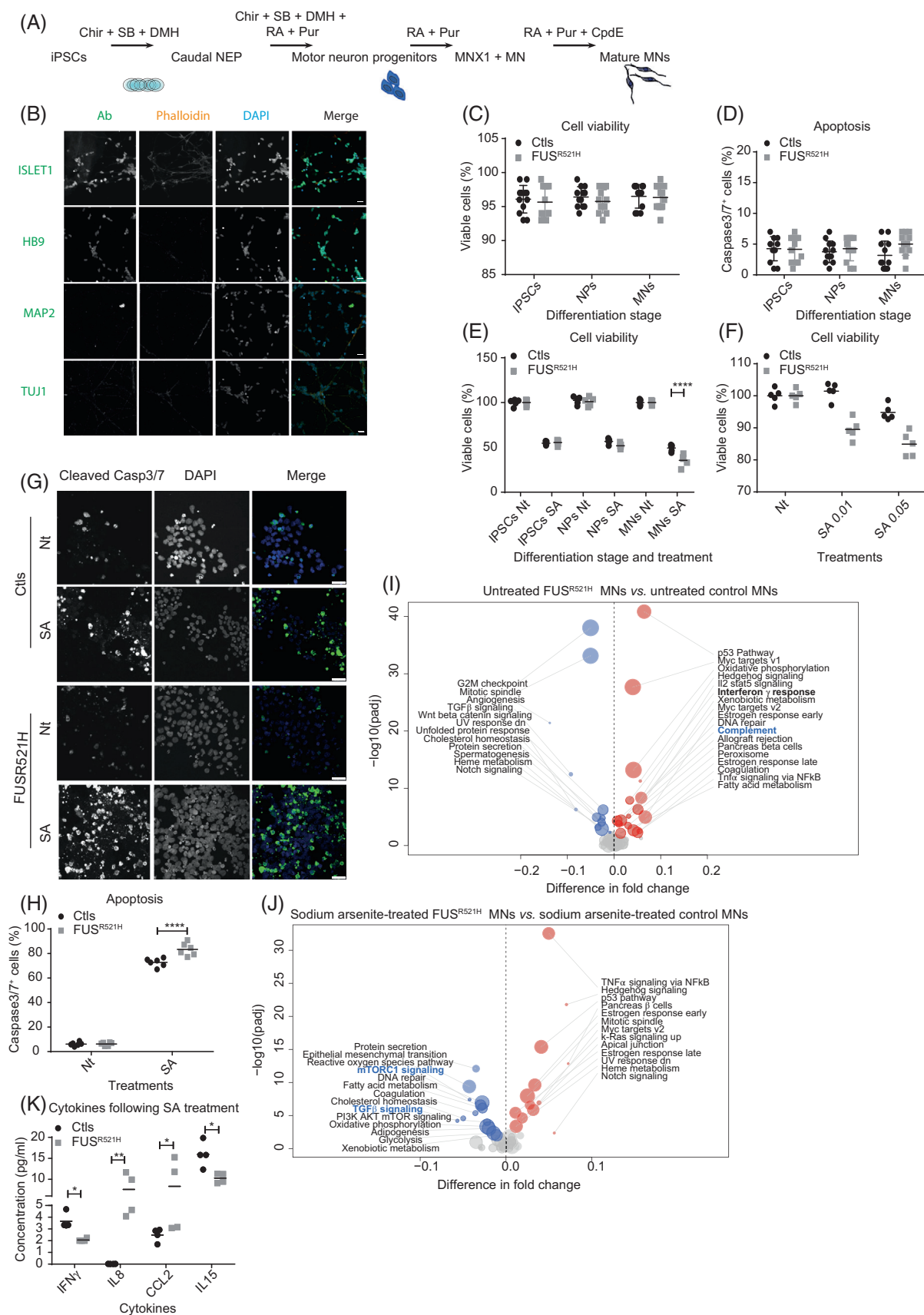


FIGURE 1 Legend on next page.

treatment and mTORC and FUS both have known roles in protein synthesis [21–23], we next assessed protein translation in iPSCs, NPs, or MNs from FUS^{R521H} patients and controls. To quantify translation rates, we used a puromycin (a tRNA mimic) incorporation assay, followed by quantification of incorporated puromycin by Western blot (WB) and IF using an anti-puromycin antibody, a commonly used assay to measure protein synthesis rates (Figure 2A–C) [24]. While protein synthesis rates were similar between all iPSC samples, untreated FUS^{R521H} NPs and MNs displayed significantly decreased translation rates compared to untreated control NPs and MNs. This was not the case when comparing treated FUS^{R521H} to control MNs, possibly because translation rates were already low in FUS^{R521H} MNs, to begin with (Figure 2D, E). We also tested whether transcription rates were affected in ALS6 cells but found no overt differences compared to wild-type cells in iPSCs, NPCs nor MNs (Figure 2A, B). These observations indicate that untreated FUS^{R521H} MNs display a translation defect, in agreement with findings of others [23, 25, 26].

To determine whether the abnormalities in the FUS^{R521H} MNs are the result of a gain-of-function mutation in the FUS gene or the result of reduced levels of functional FUS protein, we next modulated wild-type FUS or mutant FUS^{R521H} levels in control and FUS^{R521H} MNs by transient overexpression and RNA interference (Figure S2C, D). We found that overexpression of wild-type FUS in FUS^{R521H} cells nor downregulation of FUS in control MNs affected protein translation rates (Figure S2E–H). However, when we transiently overexpressed mutant FUS^{R521H} in control MNs, we did observe significantly decreased translation rates (Figure S2I, J). These data strongly suggest that the decreased translation rates observed in ALS MNs result from a gain-of-function mutation and not reduced levels of FUS functional protein. Overall, these observations suggest that FUS^{R521H} MNs are more susceptible to apoptosis due to decreased protein synthesis rates caused by an R521H gain-of-function mutation in the FUS gene.

2.4 | FUS is mislocalized into the cytoplasm in FUS^{R521H} MNs and interacts with proteins of the translational machinery in the cytoplasm

To better understand how mutant FUS leads to decreased translation, we next compared (mutant) FUS interactors between control and FUS^{R521H} MNs. For this, we co-immunoprecipitated (co-IPed) endogenous wild type and/or mutant FUS from FUS^{R521H} and control MNs followed by proteomic shotgun identification of the protein interactors (Figure 3A–C). Interestingly, co-IPed (mutant) FUS in FUS^{R521H} samples had a higher number of protein interactors compared to FUS isolates from control samples (Figure 3A; Table S1). Interestingly, FUS binding partners unique to the FUS^{R521H} isolates were enriched for proteins involved in translation initiation that are localized in the cytoplasm (Figure 3B, C). Note that the increased number of interactors in FUS^{R521H} MNs was not the result of increased expression of FUS as we observed no significant differences in FUS protein levels between wild-type and ALS6 cells across differentiation stages (Figure 3D, E).

Even though FUS is known to shuttle between the nucleus and cytoplasm in healthy cells, in ALS, FUS becomes predominantly cytoplasmic in MNs, ultimately leading to FUS aggregates [27]. Indeed, when we assessed FUS localization in FUS^{R521H} iPSCs, NPs, and MNs, we found that FUS levels were reduced in the nuclei and modestly increased in the cytoplasm of NPCs and MNs, but not iPSCs (Figure 3F, G). Wild-type iPSCs and NPCs mostly showed nuclear FUS as expected. Control MNs showed a reduction in nuclear FUS compared to iPSCs and NPCs, which was further reduced in FUS^{R521H} MNs, evidenced from IF stainings as well as WBs of cytoplasmic and nuclear fractions of MNs (Figure 3F–I).

As FUS has also been reported to be mislocalized in the cytoplasm of postmortem neurons from sporadic ALS patients [12], we next assessed FUS localization in MNs generated from iPSCs from patients with other ALS subtypes, including MNs from ALSp1, ALSp2, ALSp3, and ALSp4 patients. Also, here, we detected reduced nuclear FUS levels compared to healthy controls

FIGURE 1 FUS^{R521H} motor neurons are more sensitive to oxidative stress than control motor neurons (MNs). (A). Schematic representation of the differentiation protocol used to obtain MNs. (B) Representative images from immunofluorescence stainings to characterize MNs following the differentiation protocol. Scale bar represents 20 μ m. (C) MTS assays of untreated iPSCs, NPs and MNs 24 h following plating ($n = 6$ differentiation experiments for each individual). (D) Percentage of Caspase 3/7-positive untreated iPSCs, NPs and MNs 24 h after plating ($n = 5$ differentiation experiments for each individual). (E), (F) MTS assays of control- (Nt) or SA-treated iPSCs, NPs and MNs (E) or control or FUS^{R521H} MNs treated with different doses of SA (F) 24 h after plating. (G) Representative images from immunofluorescence stainings for Caspase3/7 of control- (Nt) or SA-treated MNs. MNs were treated for 24 h. Scale bar represents 25 μ m. (H) Percentage of Caspase 3/7-positive control- (Nt) or SA-treated MNs. Cells were treated for 24 h. (I) Volcano plot showing differentially regulated Hallmark pathways between untreated ALS and control MNs. $n = 1$ differentiation experiment for each individual. (J) Volcano plot showing differentially regulated Hallmark pathways between SA-treated FUS^{R521H} and control MNs. $n = 1$ differentiation experiment for each individual. (K) Quantification of cytokines secreted by SA-treated MNs. Cells were treated for 24 h. * = $p < 0.05$; ** = $p < 0.01$; and *** = $p < 0.001$, two-way ANOVA with Tukey multiple comparison test; $n = 2$ differentiation experiment for each individual. For all panels, each point on the graphs represents the result of one independent differentiation experiment, unless specifically stated. For statistical analysis and simplification of visualization, data from both individuals within each group were combined. Panels that do not state the number of differentiation experiments include three different biological replicates for each individual.

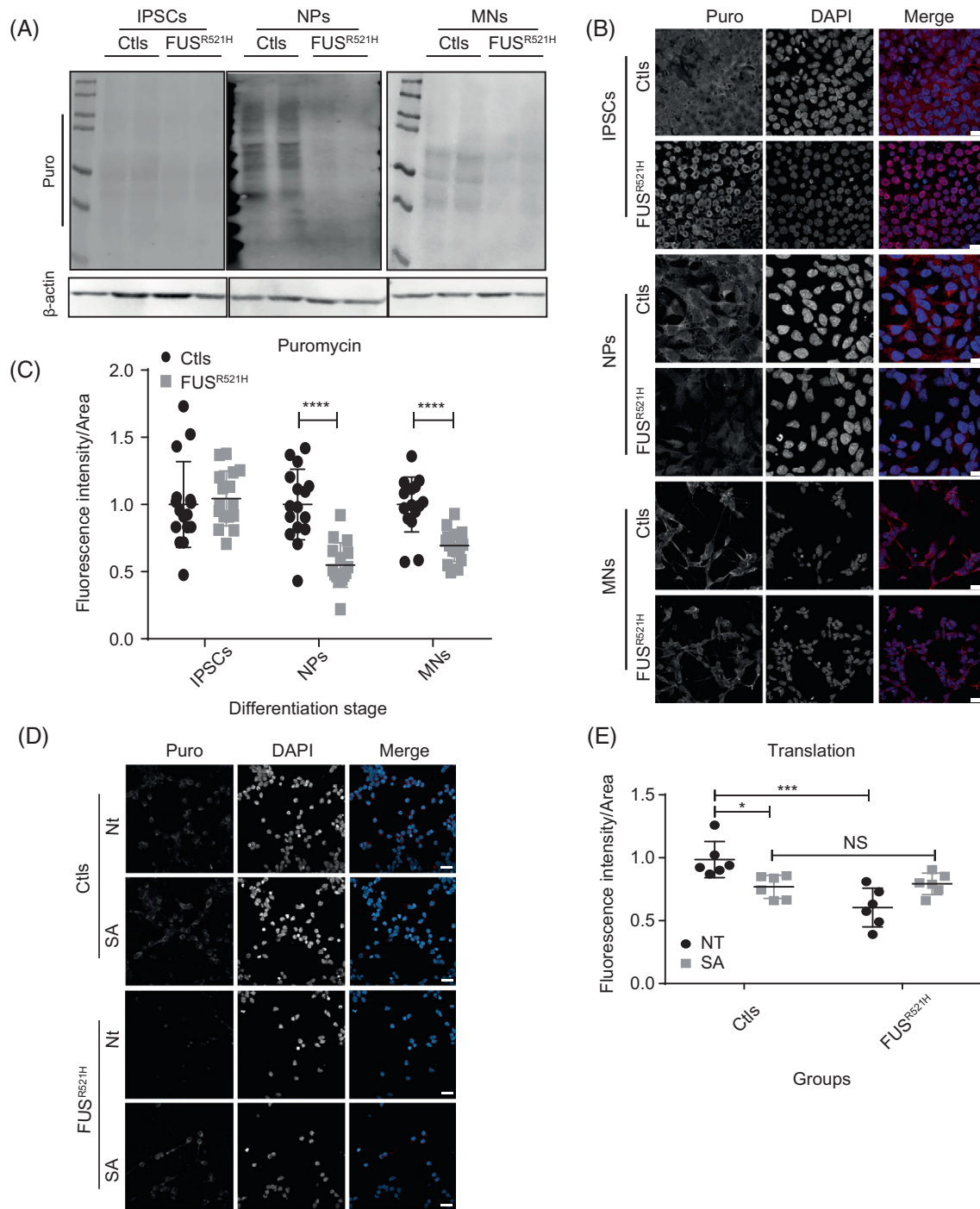


FIGURE 2 Global translation rates are decreased in FUS^{R521H} cells. (A) Western blot with anti-puromycin antibody on total cell extract of IPSCs, NPs and MNs. (B) Representative images of immunofluorescence stainings of incorporated puromycin into IPSCs, NPs and MNs. Scale bar for IPSCs represents 20 and 10 μ m for NPs and MNs. (C) Quantification of the relative intensity of puromycin incorporation in immunofluorescence stainings on IPSCs, NPs and MNs. **** = $p < 0.0001$; two-way ANOVA with Sidak's multiple comparison test; $n = 8$ differentiation experiments for each individual. (D) Representative images of immunofluorescence stainings of incorporated puromycin antibody into control- or SA-treated MNs treated with Nt or SA. Scale bar represents 10 μ m. (E) Quantification of the relative intensity of puromycin incorporation from immunofluorescence stainings on control- or SA-treated MNs. * = $p < 0.05$; *** = $p < 0.001$, two-way ANOVA with Sidak's multiple comparison test. For all panels, each point on the graphs represents the result of one independent differentiation experiment, unless specifically stated. For statistical analysis and simplification of visualization, data from both individuals within each group were combined. Panels that do not state the number of differentiation experiments include three different biological replicates each individual.

(Figure S3A, B), suggesting that aberrant FUS localization is not unique to ALS6 patients. We also compared translation rates of these cells to control cells and found

that translation rates were significantly decreased in MNs-derived from ALSp1-4 compared to healthy controls (Figure S3C, D). Together these findings suggest

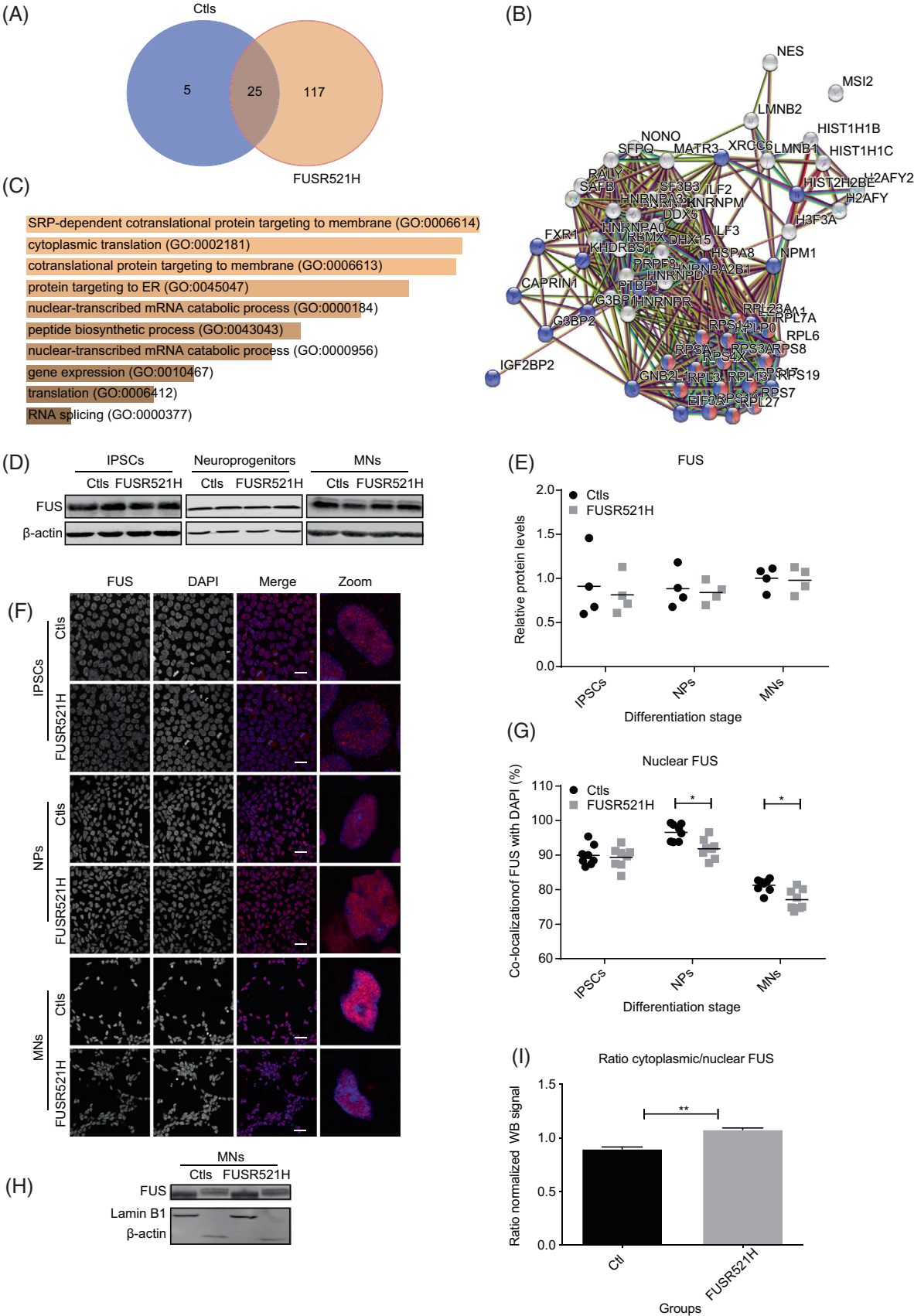


FIGURE 3 Legend on next page.

that aberrant cytoplasmic localization of FUS is common among ALS subtypes and leads to promiscuous binding of FUS to cytoplasmic proteins with a role in translation.

2.5 | IFN γ treatment or FUS knockdown rescue motor neuron viability following sodium arsenite treatment

As cytokine measurements showed reduced secreted IFN γ in FUS^{R521H} MNs treated with SA, and we recently found that inflammatory cytokines can protect cells from stress-induced cell death [28], we tested whether this was also true for FUS^{R521H} MNs. For this, we supplemented SA-treated FUS^{R521H} MNs with IFN γ and found that this indeed increased viability of FUS^{R521H} MNs to levels similar to SA-treated control MNs (Figure 4A, B). Furthermore, IFN γ treatment reduced the fraction of apoptotic FUS^{R521H} MNs following SA exposure (Figure 4C, D, Figure S4A; data presented for individual experiments); Figure S4B (data for additional iPSC lines). Importantly, we also found that IFN γ treatment resulted in an increased IFN γ transcriptional response in SA-treated FUS^{R521H} MNs (Figure 4E), indicating that IFN γ treatment was sufficient to rescue the impaired IFN γ response observed in SA-treated FUS^{R521H} MNs (compare Figure S1B to Figure 4E).

As FUS^{R521H} MNs showed impaired translation rates and these coincide with increased sensitivity to SA treatment, we next determined whether IFN γ treatment improved translation rates in FUS^{R521H} MNs. Translation rates were lower in FUS^{R521H} cells not exposed to SA, in agreement with our own findings (Figure 2) and those of others [23, 26]. Intriguingly, while IFN γ treatment did not affect translation rates in treated and untreated control MNs, it significantly increased translation rates in untreated as well as SA-treated FUS^{R521H} MNs (Figure 4F, G) Figure S4C (data presented for individual experiments); Figure S4D (data for additional iPSC lines), in line with our observation that IFN γ treatment leads to increased expression of genes involved in mTORC signaling (Figure 4E). Therefore, we investigated the effect of IFN γ on FUS localization and found

that IFN γ treatment increased nuclear localization of FUS almost to levels in control MNs (Figure S4E, F). Together, these results indicate that IFN γ treatment of FUS^{R521H} MNs improves their disease phenotype and decreases their sensitivity to SA, suggesting that ALS6 patients could benefit from IFN γ treatment to delay disease onset and/or progression.

Finally, since IFN γ treatment increased nuclear localization of FUS and ameliorated MNs survival, we investigated whether siRNA-mediated knockdown of FUS would improve translation rates and thus decrease the sensitivity to SA of FUS^{R521H} MNs. Indeed, we observed that FUS knockdown improved translation rates in FUS^{R521H} MNs to levels comparable to control MNs (Figures 5A, B S4G; data presented for individual siRNAs); Figure S4H (data for additional iPSC lines). Furthermore, FUS knockdown decreased the percentage of caspase-positive cells following SA treatment (Figure 5C, D Figure S5A; data presented for individual siRNAs); Figure S5B (data for additional iPSC lines). Together, these findings demonstrate that knockdown of FUS ameliorates the phenotype of ALS MNs similar to IFN γ treatment in agreement with findings of others [29].

Altogether our findings suggest that IFN γ treatment either or not in combination with FUS silencing could be a therapeutic strategy to treat FUS-dependent ALS.

3 | DISCUSSION

In this study, we identify IFN γ as a potential compound to protect FUS^{R521H} MNs from oxidative stress. FUS is ubiquitously expressed and shuttles between the cytoplasm and nucleus in different cell types, but in healthy neurons FUS is mainly localized in the nucleus [30]. In addition to the role of FUS in transcription and splicing, FUS also plays a role as an mRNA transporter between the nucleus and cytoplasm, for instance in neuronal dendrites to transport mRNA into dendritic spines, which is critical for neuronal maturation [31]. Cytoplasmic mislocalization and thus reduced nuclear FUS is a well-known hallmark of ALS. Indeed, more than 50% of FUS mutations are clustered near the C-terminal NLS domain, underscoring the

FIGURE 3 FUS localizes into the cytoplasm in FUS^{R521H} cells and interacts with cytoplasmic proteins of the translational machinery. $n = 1$ differentiation experiment for each individual. (A) Venn diagram of proteins interacting with FUS in each sample type. (B) String association diagram of FUS interacting proteins unique to FUS^{R521H} samples. (C) Panther bar graph of enriched pathways in FUS interacting proteins unique to FUS^{R521H} samples. (D) Western blot of total FUS protein levels in iPSC, NP, and MNs samples. (E) Densitometric quantification of the total amount of FUS in each sample relative to β -Actin ($n = 2$ differentiation experiments for each individual). (F) Representative images of immunofluorescence stainings of FUS showing nuclear localization in control and nuclear localization in all cells and partial and cytoplasmic localization in FUS^{R521H} MNs Scale bar represents 10 μ m. (G) Quantification of FUS localization from immunofluorescence stainings as shown in (F) in control and FUS^{R521H} iPSCs, NPs and MNs. * = $p < 0.05$; two-way ANOVA with Sidak's multiple comparison test; ($n = 4$ differentiation experiments for each individual). (H) Western blot for FUS protein in nuclear and cytoplasmic fractions of control and FUS^{R521H} MNs. Lamin serves as a nuclear control and Actin as a cytoplasmic control. (I) Quantification of the ratio between cytoplasmic and nuclear FUS determined from Western blots ($n = 1$ differentiation experiment for each individual) as shown in (H). For all panels, each point on the graphs represents the result of one biological replicate, unless specifically stated. For statistical analysis and simplification of visualization, data from both individuals within each group were combined. Panels that do not state the number of differentiation experiments include three biological replicates for each individual.

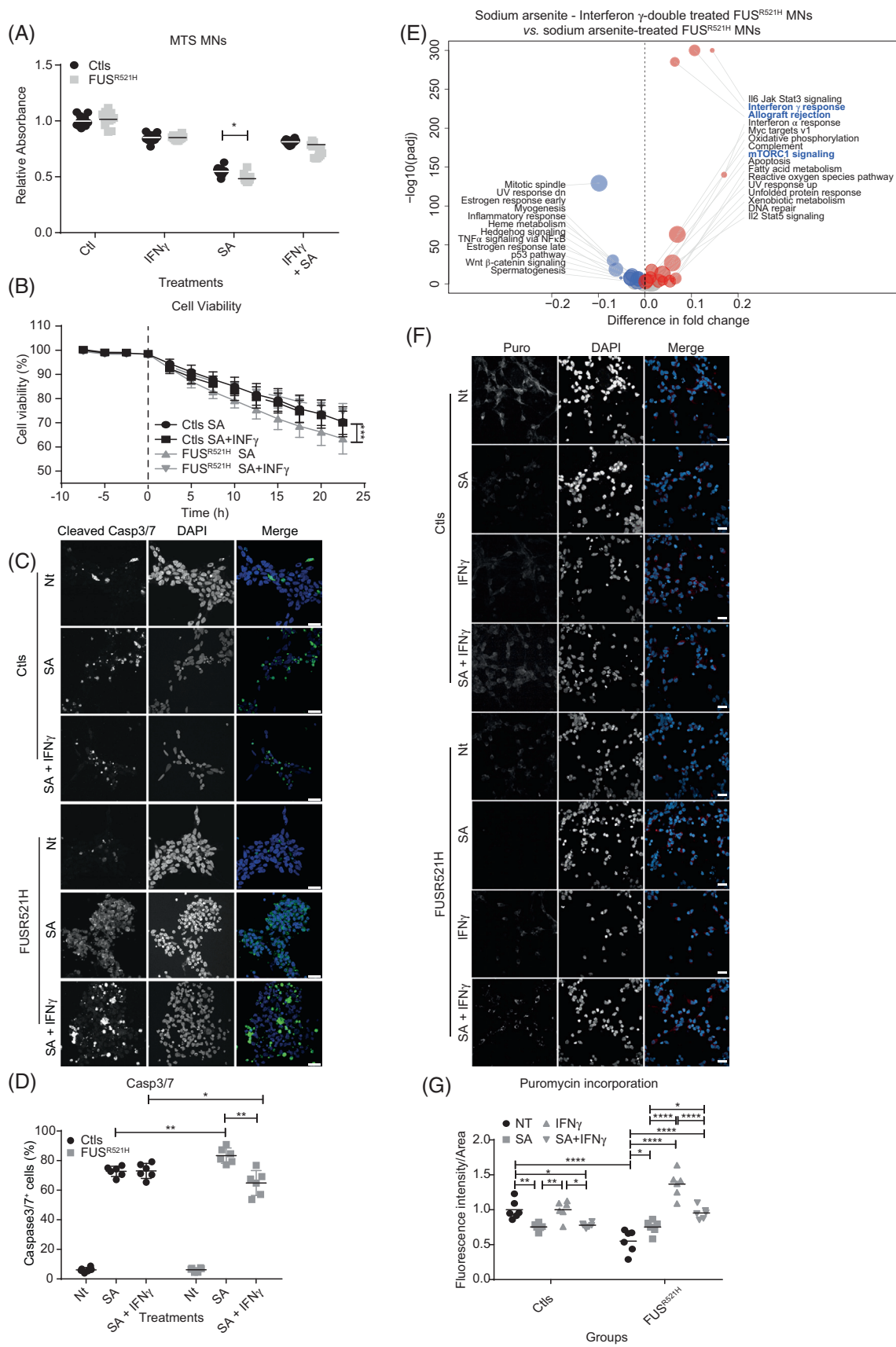


FIGURE 4 Legend on next page.

importance of defective nuclear import and the resulting enhanced cytoplasmic localization phenotype for the pathobiology of ALS [4].

To investigate the effect of the FUS^{R521H} mutation, common to ALS6, we used patient-derived iPSC models and generated MNs to study the disease biology in a highly physiological setting. It is important to note here that we used siblings-derived iPSCs instead of generating isogenic iPSC lines, for instance using CRISPR engineering. While our findings provide valuable insights into the effect of the ALS6 FUS^{R521H} mutation on MNs, it will be important to confirm our findings using such isogenic iPSC lines. In addition, since we only derived two control- and two patient-derived lines, validation of our findings in additional patients-derived iPSC lines will be required to generalize our results.

Interestingly, although we find modest transcriptional differences between healthy control and FUS^{R521H} MNs, the viability of untreated FUS^{R521H} MNs is identical to control MNs, suggesting that both cultures manage to achieve homeostasis. However, as reprogramming somatic cells into iPSCs coincides with cellular rejuvenation, our MN model could well be recapitulating young MNs, while ALS (6) symptoms typically present later in life. To model age-associated damage, we, therefore, added an oxidative stress component to our model system by exposing the cells to SA [18, 32]. Furthermore, increased oxidative stress and ROS accumulation has been extensively reported as a hallmark of ALS as ROS are byproducts of cellular respiration as neurons have higher metabolic rates and transcriptional activity [33]. Indeed, we find that MNs carrying the FUS^{R521H} mutation are more sensitive to SA treatment than matched control MNs consistent with previous studies [7].

We used RNA-seq to comprehensively evaluate the impact of FUS^{R521H} mutation on ROS sensitivity in untreated and SA-treated MNs. We find increased expression of innate immune system components in untreated mutant cells, suggesting that FUS^{R521H} MNs exhibit intrinsic inflammation, in accordance with several lines of evidence suggesting toxic effects of the inflammatory response during disease progression [34–38]. We also find that FUS^{R521H} MNs display a lower expression of

genes in the TGF- β signaling pathway following SA treatment. This is quite interesting as TGF- β signaling has been described as neuroprotective following oxidative stress [39–41] and suggests that the failure of ALS to induce TGF- β following SA might be related to the increased sensitivity to SA-induced oxidative stress. Furthermore, cytokines measurements show that SA-treated FUS^{R521H} MNs secrete more IL-8 and CCL2, and less IL-15 and IFN γ compared to SA-treated control MNs. This is interesting, as other studies have reported elevated levels of IL-15 and IFN γ in serum and CSF of sporadic ALS patients [42, 43]. It is important to note here that we quantified cytokine secretion from MNs directly, while these other studies measured cytokines in serum, which might not fully represent what happens nearby the MNs. However, future work using iPSC-derived MNs modeling other subtypes of ALS should reveal whether the decreased secretion of IL-15 and IFN γ by MNs is specific to FUS^{R521H} patients or a feature more general to (sporadic) ALS MNs.

It is still not fully clear whether the FUS^{R521H} mutation and its cytoplasmic localization result from a gain-of-toxicity or loss-of-function effect in the FUS protein. Our results are consistent with previous studies suggesting that the FUS^{R521H} mutation leads to a gain of function that impairs protein translation [26, 44–46] as we have identified a large number of FUS protein–protein interactors unique to the FUS^{R521H} cells. We find that these interactors have a function in translation initiation and are localized in the cytoplasm. Furthermore, studies in humanized mice expressing FUS^{R521H} showed an activated stress response and impaired local intra-axonal protein synthesis in hippocampal neurons and sciatic nerves without nuclear loss of function [23].

We also observed that a small fraction of the FUS^{R521H} protein localizes to the cytoplasm, consistent with studies showing mild cytoplasmic localization of mutant FUS^{R521G}, FUS^{R521H} and FUS^{R521C} protein [9], suggesting that mild cytoplasmic localization of FUS is sufficient to disrupt cellular protein synthesis homeostasis. We show that this cytoplasmic localization in MNs is not unique to ALS MNs with mutations in FUS but also occurs in MNs derived from iPSCs of patients with

FIGURE 4 IFN γ treatment rescues oxidative stress-induced decreased viability of FUS^{R521H} MNs. (A) Cell viability of control (Nt), SA, IFN γ or combination-treated control and FUS^{R521H} MNs assessed by the MTS assays. *** = $p < 0.001$, two-way ANOVA with Tukey multiple comparison test; ($n = 4$ differentiation experiments for each individual). (B) Cell viability of control (Nt), SA, IFN γ or combination-treated control and FUS^{R521H} MNs assessed by xCELLigence real-time cell analysis system. *** = $p < 0.001$, two-way ANOVA with Tukey multiple comparison test; $n = 4$ differentiation experiments for each individual. (C) Representative images of immunofluorescence stainings for Caspase3/7 on control (Nt), SA, IFN γ or combination-treated MNs. Cells were treated for 24 h. Scale bar represents 25 μ m. (D) Percentage of Caspase 3/7-positive control (Nt), SA, IFN γ or combination-treated MNs. Cells were treated for 24 h. * = $p < 0.05$; ** = $p < 0.01$; and *** = $p < 0.001$, two-way ANOVA with Tukey multiple comparison test. (E) Volcano plot showing differentially regulated Hallmark pathways between SA + IFN γ FUS^{R521H} and SA-treated MNs. (F) Representative images of immunofluorescence staining for incorporated puromycin in MNs for the four following treatments: Control (Nt), IFN γ , SA, and SA + IFN γ . Scale bar represents 20 μ m. (G) Relative intensity of puromycin incorporation from immunofluorescence stainings for puromycin incorporation into MNs for the four following treatments: Control (Nt), IFN γ , SA, and SA + IFN γ . * = $p < 0.05$; ** = $p < 0.01$; and *** = $p < 0.001$, two-way ANOVA with Tukey multiple comparison test. For all panels, each point on the graphs represents the result of one biological replicate, unless specifically stated. For statistical analysis and simplification of visualization, data from both individuals within each group were combined. Panels that do not state the number of differentiation experiments include three different biological replicates for each individual.

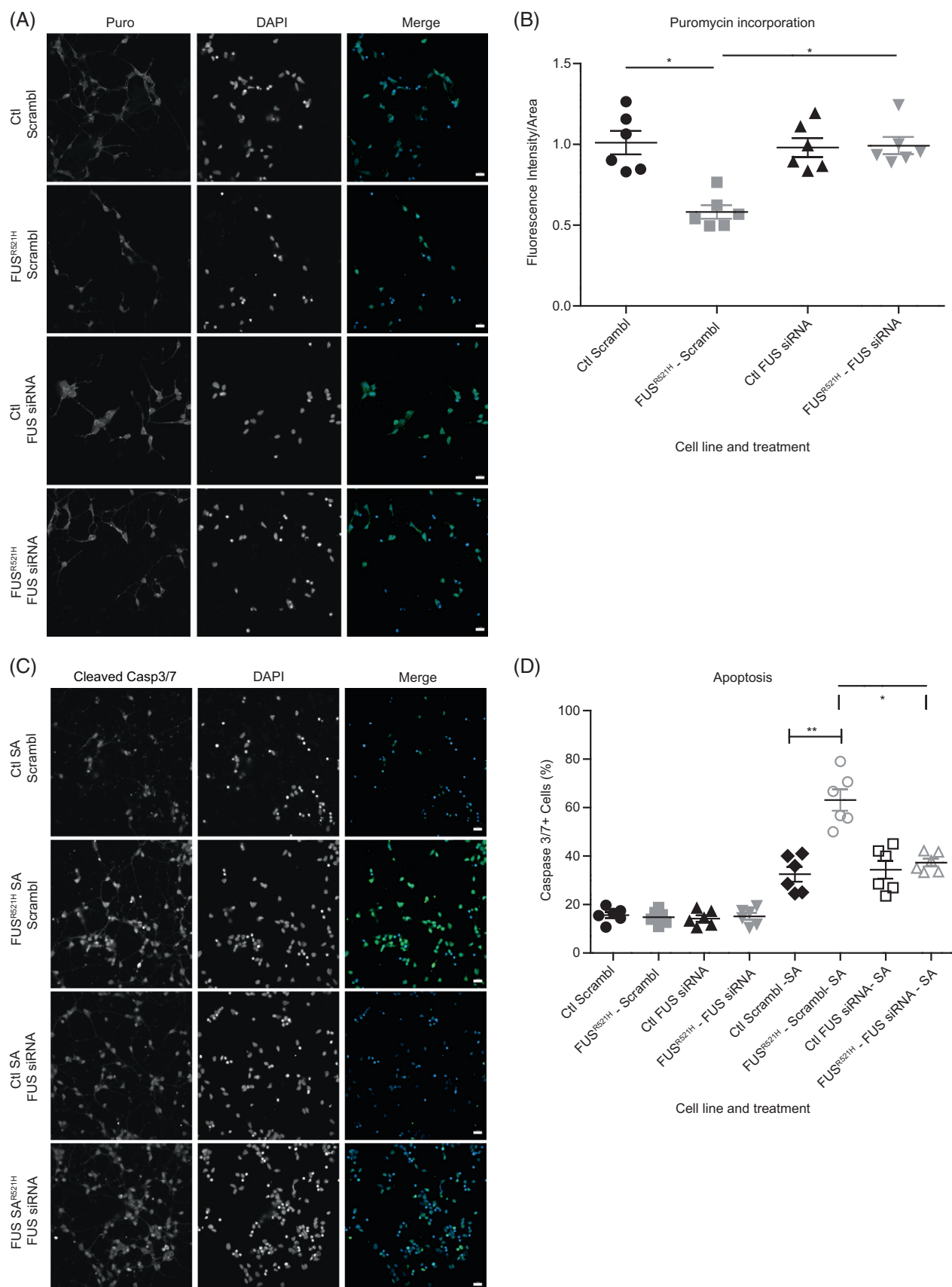


FIGURE 5 Legend on next page.

familial forms of ALS linked to mutations in the VAPB and VRK1 genes. In agreement with this, these MNs also displayed decreased translational rates. Therefore, our findings are consistent with other studies that suggest that mutant FUS represses translation through association with polyribosomes [47].

When we treated FUS^{R521H} MNs with IFN γ following the induction of ROS, we found that IFN γ -treated FUS^{R521H} MNs are less sensitive to SA-induced ROS. Intriguingly, IFN γ treatment also led to decreased cytoplasmic localization of FUS and increased protein translation rates, suggesting that IFN γ treatment decreases the impact of ROS somewhere upstream in the stress signaling cascade. There is conflicting evidence regarding the relationship between neurons and IFNs, as both protective as well as detrimental effects of IFNs have been suggested for ALS neurons [48–51]. For instance, it has recently been shown that IFN γ stimulation of adult human astrocytes yields neurotoxicity in vitro [48]. Furthermore, studies with high doses of IFN α in ALS patients result in cognitive decline, memory and psychomotor impairment, neurotoxicity and other side effects [51–53]. Conversely, both IFN- β 1b and IFN- β 1a treatments were found to inhibit the pro-inflammatory cytokines (IL-6, IL-1 β , TNF- α , and IFN- γ), increase the myelin protein level in the brain cortex, and improve the neurological status of experimental autoimmune encephalomyelitis rats [50]. Finally, IFN β treatment in ALS patients has not shown any significant difference between patients given IFN β -1a and patients given a placebo [49]. Therefore, while our work suggests a positive effect of IFN γ treatment, at least for ALS6 patients, further work is needed to compare the exact role of individual interferon signaling components between various ALS and control neuronal cell types.

Altogether, our work indicates that FUS^{R521H} MNs are more sensitive to SA-induced oxidative stress compared to control MNs and that IFN γ improves survival, specifically of FUS^{R521H} MNs. This IFN γ -mediated rescue coincides with increased translation rates and decreased cytoplasmic localization of mutant FUS. While further work is required to disentangle the exact underlying molecular mechanism of this rescue, our findings might suggest that IFN γ , when dosed timely and appropriately, could protect MNs in ALS6 patients and might thus delay disease onset or

progression. However, before testing this in patients, further work is required, such as validating the neuroprotective effects of IFN γ treatment in ALS6-mouse models [23] or, possibly in patient-derived MN models that better recapitulate the effects of natural aging, for instance by direct conversion of neurons from fibroblasts isolated from patients presenting ALS symptoms [54], or by overexpressing ageing-inducing factors such as Progerin [55].

4 | EXPERIMENTAL PROCEDURES

4.1 | Patient material

Fibroblasts from patients and unaffected family members (Table 1) were collected at the Centro de Pesquisas sobre o Genoma Humano e Células-Tronco. Sampling was approved by the Comitê de Ética em Pesquisa do Instituto de Biociências da Universidade de São Paulo – IBUSP #5464/Certificate CAAE # 20108413.4.0000.5464.

4.2 | Cellular reprogramming, characterization and motor neuron differentiation

Fibroblasts were reprogrammed using CytoTune™-iPS 2.0 Sendai Reprogramming Kit (Thermo) as per

TABLE 1 Sex and age at time of collection of fibroblasts from patients and unaffected family members.

Individual code	Sex	Age at sample collection
Control 1	Male	44
Control 2	Female	42
R521H FUS 1	Male	41
R521H FUS 2	Male	52
ALS p1 (p56sVAPB)	Male	54
ALS p2 (p56sVAPB)	Female	52
ALS p3 (VRK1 locus—to be confirmed)	Female	43
ALS p4 (VRK1 locus—to be confirmed)	Male	42

FIGURE 5 FUS knockdown rescues translation and apoptosis rates of FUS^{R521H} MNs. (A) Representative images of immunofluorescence staining for incorporated puromycin in MNs for the four following treatments: Control (Scramble siRNA), FUS^{R521H} (Scramble siRNA), Control (FUS siRNA) and FUS^{R521H} (FUS siRNA). Scale bar represents 20 μ m. (B) Relative intensity of puromycin incorporation in MNs from immunofluorescence stainings for the four following treatments: Control (Scramble siRNA), FUS^{R521H} (Scramble siRNA), Control (FUS siRNA) and FUS^{R521H} (FUS siRNA). * = $p < 0.05$; two-way ANOVA with Tukey multiple comparison test. (C) Representative images of immunofluorescence stainings for Caspase3/7 on SA-treated Control (Scramble siRNA), FUS^{R521H} (Scramble siRNA), Control (FUS siRNA) and FUS^{R521H} (FUS siRNA). Cells were treated for 24 h. Scale bar represents 20 μ m. (D) Percentage of Caspase 3/7-positive on not treated- (Nt) or on SA-treated Control (Scramble siRNA), FUS^{R521H} (Scramble siRNA), Control (FUS siRNA) and FUS^{R521H} (FUS siRNA). Cells were treated for 24 h. * = $p < 0.05$; ** = $p < 0.01$; two-way ANOVA with Tukey multiple comparison test. For all panels, each point on the graphs represents the result of one independent differentiation experiment, unless specifically stated. For statistical analysis and simplification of visualization, data from both individuals within each group were combined. Panels that do not state the number of differentiation experiments include 3 different biological replicates for each individual.

manufacturer instructions. iPSCs were cultured in Essential 8 medium (Thermo). iPSCs clones euploidy was analyzed by Chromosomal microarray analysis using the customized array-CGH 180k Agilent platform. Agilent Genomic Workbench software was used to call CNVs. Pluripotency markers were checked by immunofluorescence using anti OCT4, SOX2 and NANOG antibodies (Figure S1C). MN's differentiation was performed as previously described [16]. Briefly, iPSCs were cultured in NB medium containing DMEM/F12, Neurobasal medium, N2, B27 and Glutamax (Thermo). Differentiation was performed using a two-step protocol: neural induction and caudalization and ventralization to obtain motor neuron progenitors (MNP's). For this, iPSCs were cultured for 6 days in NB medium with Dorsomorphin (2 μ M) (Sigma), SB431542 (2 μ M) (Sigma), CHIR99021 (3 μ M) (Tocris) and Ascorbic acid (0.1 mM) (Sigma) for neural induction followed by a six-day culture in NB medium containing Dorsomorphin (2 μ M) (Sigma), SB431542 (2 μ M) (Sigma), CHIR99021 (1 μ M) (Tocris), retinoic acid (0.1 μ M) (Sigma), Ascorbic acid (0.1 mM) (Sigma) and Purmorphamine (0.5 μ M) (Tocris) for caudalization and ventralization of MNP's. MNP's were seeded in 60 mm² plates coated with Matrigel (Corning) for MN differentiation with NB medium containing retinoic acid (0.5 μ M) (Sigma), Purmorphamine (0.1 μ M) (Tocris) and Ascorbic acid (0.1 mM) (Sigma) for 6 days. For neural maturation, Compound E (0.1 μ M) (Calbiochem) was added to NB medium with retinoic acid (0.5 μ M) (Sigma), Purmorphamine (0.1 μ M) (Tocris) and Ascorbic acid (0.1 mM) (Sigma). All cells were cultured at 37°C and 5% CO₂ in a humidified incubator and routinely checked for mycoplasma infection.

4.3 | Immunofluorescence

Motor neurons were fixed with 3.7% formaldehyde (Sigma) in 1× PBS (Gibco) for 20 min at room temperature followed by a 30 min permeabilization step using 0.1% Triton X-100 (Thermo) in 5% bovine serum albumin (BSA) (Sigma). Protein labeling was done by incubation with appropriate primary antibodies as indicated (Table S2) in 5% BSA (Sigma) at 4°C overnight, followed by incubation with the appropriate fluorescent secondary antibody for 45 min. Slides were washed two times with 1× PBS (Gibco) and counterstained with 1 μ g/mL DAPI (Thermo) for 2 min to label nuclei and mounted with VectaShield (Vector Laboratories). Images were taken using a confocal microscope (Zeiss LSM 800). Quantification was performed using Cell Profiler 3.0 as previously described [56, 57].

4.4 | Immunoblotting

MNs were harvested by accutase (Gibco) dissociation and lysed with elution buffer (150 mM NaCl–Sigma,

0.1% NP-40–Sigma, 5 mM EDTA–Sigma, 50 mM HEPES–Sigma pH 7.5, and protease inhibitor cocktail–Sigma) for 15 min at 4°C and centrifuged for 10 min at 300 × *g* at 4°C to obtain cell lysates. Proteins were separated on a 10% polyacrylamide gel and transferred onto a polyvinylidene difluoride (PVDF) membrane (Sigma). Membranes were blocked in Odyssey blocking buffer (Li-cor Biosciences) for 60 min at 4°C. Membranes were incubated with primary antibodies overnight at 4°C as indicated. Following primary antibody incubation membranes were washed three times with 0.1% Tween 20 (Sigma) in 1× PBS (Gibco) followed by incubation with the appropriate secondary antibody for 1 h at room temperature. WBs were detected using the Odyssey imaging system (Li-cor Biosciences). Quantification of the bands was performed using Image studio lite software (Li-cor Biosciences).

4.5 | Cytokine measurements

Cytokines were quantified in media isolated from MN cultures using the Bio-Plex Pro Human Cytokine kit (Biorad, USA) according to the manufacturer's instructions. MNs were plated at a density of 5 × 10⁵ cells/well and treated with SA (5 μ M) (Sigma), IFN γ (50 ng/mL) (Peprotech), or a combination for 24 h prior to measurements.

4.6 | Co-immunoprecipitation

Co-IPs for FUS were performed using an Immunoprecipitation Kit Dynabeads Protein A/G (ThermoFisher) according to the manufacturer's protocol. Briefly, protein A/G beads were incubated with 10 μ L of the relevant antibody or mouse IgG as a control. Cells were washed once with PBS and lysed in 500 μ L/well lysis buffer containing 20 mM Tris pH 8.0, 10% glycerol, 135 mM NaCl, 0.5% NP-40, and protease inhibitors (Complete, EDTA-free, Roche) for 15 min on ice. After harvesting, cells were centrifuged at 16,100 × *g* for 5 min at 4°C to remove cell debris. The supernatant was incubated with antibody-conjugated beads for 1 h at 4°C. Following three washing steps with wash buffer, beads were taken up in RapiGest (Waters) for 10 min at 65°C.

4.7 | Liquid chromatography coupled to tandem mass spectrometry

Samples were digested using RapiGest (Waters) as a surfactant agent. Proteins were reduced with DTT (Sigma) and alkylated with iodoacetamide (Sigma). Samples were further digested with trypsin proteomic level (Promega) in enzyme: Protein ratio of 1:50. Samples were processed by nanoACQUITY system with a binary pump, an auxiliary pump and a sampler. Desalted and concentrated

peptides were captured in a Symmetry C18 column (2 nm \times 180 mm, 5 μ m) in a mobile phase (composed of water with 0.1% trifluoroacetic acid) at 15 μ L/min flow rate for 5 min. Furthermore, peptides were separated in an analytical HSSC18 column (75 μ m \times 150 mm, 1.7 μ m) by elution with a linear gradient of 2% DMSO (Sigma) in water with 0.1% formic acid (Sigma) and 5% DMSO in acetonitrile (LiChrosolv) with 0.1% formic acid. The proportion of the organic solution was increased from 0% to 60% in 80 min.

The chromatographic system was directly coupled to a hybrid quadrupole orbitrap tandem mass spectrometer Q-Exactive (Thermo Scientific), equipped with a Nano Flex source. Acquisition of spectral data was obtained by a data-dependent top-15 method in which the spectrometer chooses dynamically the most abundant not-yet sequenced precursor ions from a survey scan from 390 to 1650 m/z (except for the monocharged and those with charges exceeding 7) at 70,000 (at m/z 200) of resolution and AGC target 5 e 6. Sequencing was achieved by dissociating the precursor ion with a normalized collision energy of 35, resolution equal to 17,500 and AGC target of 5 e 4.

Acquired data were processed using MaxQuant 1.4.0.8 proteomics data analysis workflow 27. Protein identification was performed by the Andromeda search tool using the database of the human proteome UniProtKB (SWISSPROT November 2017). The following criteria were applied for protein identification: (1) a maximum of two incomplete cleavages by trypsin, (2) fixed modification by carbamidomethylation of cysteines, and (3) variable modification by acetylation of the N-terminal portion and methionine oxidation. Quantification was based on the LFQ 28 label-free method.

4.8 | Puromycin incorporation assay

Cells were incubated with or without 20 μ M puromycin (Invitrogen) and fixed for immunofluorescence or lysed for immunoblotting.

4.9 | Subcellular fractionation

Cytoplasmic/nuclear fraction separation was performed by dissolving 3×10^6 cells in 200 μ L of cold hypotonic buffer (10 mM HEPES–NaOH pH 7.9, 10 mM KCl, 1.5 mM MgCl₂, 1 mM DTT, and protease and phosphatase inhibitors—all compounds from Sigma). Cells were incubated on ice and inverted every 5 min for 30 min, followed by centrifugation for 10 min at $400 \times g$ at 4°C. The supernatant was taken as the cytoplasmic fraction and the pellet was washed three times with a cold hypotonic buffer. Pellets were dissolved in cold 100 mM Tris–HCl (pH 9.0) containing 12 mM SDC (Sigma), 12 mM SLS (Sigma), and protease and phosphatase

inhibitors, and collected as the nuclear fraction. Both fractions were subjected to SDS-page and WB.

4.10 | EU labeling

Cells were incubated with 10 μ M EU (5-ethynyl-uridine; Click-It EU Alexa Fluor 488 Imaging Kit; Life Technologies) for 30 min. Cell nuclei were labeled with DAPI (Sigma) at a concentration of 5 μ g/mL for 5 min. Images were taken using a confocal microscope (Zeiss LSM 800). Quantification was performed using Cell Profiler 3.0 as previously described [56, 57].

4.11 | MTS assay

MTS assays were performed according to manufacturer's instructions. Briefly, 15,000 MNs were plated per well and treated with IFN γ (50 ng/mL), SA (5 μ M) and for the time indicated at relevant figures. MTS reagent (10 μ L) (Promega) was added directly to the wells and incubated at 37°C for 4 h. Absorbance was measured at 490 nm on a SpectraMax Plus 384 reader (Molecular Devices; Sunnyvale, Ca).

Cell viability assay kill curves were quantified by the impedance-based xCELLigence real-time cell analysis system (ACEA Biosciences, San Diego, CA, USA). For this, 50 μ L of cell culture media was added to each 96 wells of the E-Plate 96 PET (ACEA Biosciences) for background reading. Subsequently, 50 μ L of cell suspension containing 15,000 cells was added to each well and placed inside the xCELLigence incubator. Cells were treated with IFN γ (50 ng/mL) (Peprotech), SA (5 μ M) (Sigma) and impedance reflecting changes in cell adhesion and cell death were measured every 15 min for 24 h. Data are presented as changes of impedance ('Cell Index') over time, according to the manufacturer's instruction.

4.12 | RNA sequencing

RNA was isolated using an RNeasy mini kit (Qiagen). RNA quality and quantity of the total RNA were assessed by the 2100 Bioanalyzer using a Nano chip (Agilent, Santa Clara, CA). Total RNA samples having a RIN >8 were subjected to library generation. Strand-specific libraries were generated using the TruSeq Stranded mRNA sample preparation kit (Illumina Inc., San Diego, RS-122-2101/2), according to the manufacturer's instructions (Illumina, Part #15031047 Rev. E).

Polyadenylated RNA from intact total RNA was purified using oligo-dT beads. Following purification, the RNA was fragmented, random primed and reverse transcribed using SuperScript II Reverse Transcriptase (Invitrogen, part 72 #18064-014) with the addition of Actinomycin D. Second strand synthesis was performed

using Polymerase I and RNaseH with replacement of dTTP for dUTP. The generated cDNA fragments were 3'-end adenylated and ligated to Illumina Paired-end sequencing adapters and subsequently amplified by 12 cycles of polymerase chain reaction. Sequencing libraries were analyzed on a 2100 Bioanalyzer using a 7500 chip (Agilent, Santa Clara, CA), diluted and pooled equimolar into a 10 nM sequencing stock solution. Illumina TruSeq mRNA libraries were sequenced at a resolution of 50 base single reads on a HiSeq2000 using V3 chemistry (Illumina Inc., San Diego). Resulting reads were trimmed using Cutadapt (version 1.12) to remove any remaining adapter sequences, filtering reads shorter than 20 bp after trimming to ensure efficient mapping. The trimmed reads were aligned to the GRCh38 reference genome using STAR (version 2.5.2b). QC statistics from Fastqc (version 0.11.5) and the above-mentioned tools were collected and summarized using Multiqc (version 0.8). Gene expression counts were generated by featureCounts (version 1.5.0-post3), using gene definitions from Ensembl GRCh38 version 76. Normalized expression values were obtained by correcting for differences in sequencing depth between samples using DESeq median-of-ratios approach, and subsequent log-transformation of the normalized counts.

4.13 | Statistical analyses

Experiments were performed in at least biological triplicates as stated in the figures. Data were analyzed by one-way and two-way ANOVA followed by Bonferroni post hoc testing. A two-tailed unpaired *t*-test was used for pairwise comparison. GraphPad Prism software was used to perform all statistical analyses (version 6.0 GraphPad Software Inc.). Quantification of data is presented as mean \pm standard error of the mean (SEM), and *p*-value thresholds are presented as: * = $p < 0.05$; ** = $p < 0.01$; *** = $p < 0.001$; and **** = $p < 0.0001$.

AUTHOR CONTRIBUTIONS

Amanda F. Assoni: Conceptualization; data curation; formal analysis; validation; investigation; visualization; methodology; writing—original draft; writing—review and editing. **Erika N Guerrero:** data curation; formal analysis; visualization; writing—original draft; writing—review and editing. **René Wardenaar:** Data curation; formal analysis; investigation; methodology. **Danylo Oliveira:** Investigation, visualization; methodology. **Petra L. Bakker:** Investigation, methodology, validation. **Valdemir Melechco Carvalho:** Investigation, methodology. **Oswaldo Keith Okamoto:** Resources; data curation; formal analysis; supervision; funding acquisition. **Mayana Zatz:** Conceptualization; supervision; resources. **Floris Foijer:** Conceptualization; resources; data curation; formal analysis; supervision; funding acquisition; investigation; visualization; methodology; writing—original draft; project administration; writing—review and editing.

ACKNOWLEDGMENTS

We thank the people in the Foijer and Zatz labs for fruitful discussions. This work was supported by the Fundação de Amparo à Pesquisa do Estado de São Paulo (FAPESP), Conselho Nacional de Desenvolvimento Científico e Tecnológico (CNPq) and an Abel Tasman fellowship to AA awarded by the University of Groningen.

CONFLICT OF INTEREST STATEMENT

The authors declare no competing interests.

DATA AVAILABILITY STATEMENT

All RNA sequencing data has been deposited at ArrayExpress under accession number E-MTAB-12422. All proteomic data has been deposited at PRIDE under accession number PXD038042.

ORCID

Valdemir M. Carvalho  <https://orcid.org/0000-0002-9816-8615>

Floris Foijer  <https://orcid.org/0000-0003-0989-3127>

REFERENCES

1. Charcot J-M. Deux cas d'atrophie musculaire progressive: avec lésions de la substance grise et des faisceaux antérolatéraux de la moelle épinière. Paris: Masson 1869.
2. Mathis S, Goizet C, Soulages A, Vallat J-M, le Masson G. Genetics of amyotrophic lateral sclerosis: a review. J Neurol Sci [Internet]. 2019 [cited 2019 Apr 10];399:217–26. Available from: <https://www.sciencedirect.com/science/article/pii/S0022510X19301017?via%3Dihub#bb0025>
3. Xu L, Liu T, Liu L, Yao X, Chen L, Fan D, et al. Global variation in prevalence and incidence of amyotrophic lateral sclerosis: a systematic review and meta-analysis. J Neurol. 2020;267:944–53.
4. Guerrero EN, Wang H, Mitra J, Hegde PM, Stowell SE, Liachko NF, et al. TDP-43/FUS in motor neuron disease: complexity and challenges. Prog Neurobiol. 2016;145–146:78–97.
5. Vance C, Rogelj B, Hortobágyi T, de Vos KJ, Nishimura AL, Sreedharan J, et al. Mutations in FUS, an RNA processing protein, cause familial amyotrophic lateral sclerosis type 6. Science. 1979;2009(323):1208–11.
6. Wang H, Rangaswamy S, Kodavati M, Mitra J, Guo W, Guerrero EN, et al. RT2 PCR array screening reveals distinct perturbations in DNA damage response signaling in FUS-associated motor neuron disease. Mol Brain [Internet]. 2019 [cited 2022 Oct 10];12:1–5. Available from: <https://molecularbrain.biomedcentral.com/articles/10.1186/s13041-019-0526-4>
7. Wang H, Guo W, Mitra J, Hegde PM, Vandoorne T, Eckelmann BJ, et al. Mutant FUS causes DNA ligation defects to inhibit oxidative damage repair in amyotrophic lateral sclerosis. Nat Commun. 2018 [cited 2022 Oct 10];9:1–18. Available from: <https://www.nature.com/articles/s41467-018-06111-6>
8. Blair IP, Williams KL, Warraich ST, Durnall JC, Thoeng AD, Manavis J, et al. FUS mutations in amyotrophic lateral sclerosis: clinical, pathological, neurophysiological and genetic analysis. J Neurol Neurosurg Psychiatry. 2010;81:639–45.
9. Vance C, Scotter EL, Nishimura AL, Troakes C, Mitchell JC, Kathe C, et al. ALS mutant FUS disrupts nuclear localization and sequesters wild-type FUS within cytoplasmic stress granules. Hum Mol Genet [Internet]. 2013 [cited 2022 Oct 10];22:2676–88. Available from: <https://pubmed.ncbi.nlm.nih.gov/23474818/>
10. Notaro A, Messina A, la Bella V. A deletion of the nuclear localization signal domain in the FUS protein induces stable post-stress

- cytoplasmic inclusions in SH-SY5Y cells. *Front Neurosci*. 2021; 15:1786.
11. Shang Y, Huang EJ. Mechanisms of FUS mutations in familial amyotrophic lateral sclerosis. *Brain Res*. 2016;1647:65–78.
 12. Tyzack GE, Luisier R, Taha DM, Neeves J, Modic M, Mitchell JS, et al. Widespread FUS mislocalization is a molecular hallmark of amyotrophic lateral sclerosis. *Brain*. 2019;142:2572–80.
 13. Nathani D, Spies J, Barnett MH, Pollard J, Wang M-X, Sommer C, et al. Nerve biopsy: current indications and decision tools. *Muscle Nerve* [Internet]. 2021 [cited 2021 Oct 18];64:125–39. <https://doi.org/10.1002/mus.27201>
 14. Lapasset L, Milhavel O, Prieur A, Besnard E, Babled A, Aït-Hamou N, et al. Rejuvenating senescent and centenarian human cells by reprogramming through the pluripotent state. *Genes Dev* [Internet]. 2011 [cited 2022 Oct 10];25:2248–53. Available from: <https://pubmed.ncbi.nlm.nih.gov/22056670/>
 15. Albers DS, Flint Beal M. Mitochondrial dysfunction and oxidative stress in aging and neurodegenerative disease. *J Neural Transm Suppl* [Internet]. 2000 [cited 2022 Oct 10];59:133–54. Available from: <https://pubmed.ncbi.nlm.nih.gov/10961426/>
 16. Du Z-W, Chen H, Liu H, Lu J, Qian K, Huang C-L, et al. Generation and expansion of highly pure motor neuron progenitors from human pluripotent stem cells. *Nat Commun* [Internet]. 2015 [cited 2019 Feb 7];6:6626 Available from: <http://www.nature.com/articles/ncomms7626>
 17. Richard JP, Maragakis NJ. Induced pluripotent stem cells from ALS patients for disease modeling. *Brain Res* [Internet]. 2015 [cited 2022 Oct 11];1607:15–25. Available from: <https://pubmed.ncbi.nlm.nih.gov/25436299/>
 18. Baron DM, Kaushansky LJ, Ward CL, Sama RRR, Chian RJ, Boggio KJ, et al. Amyotrophic lateral sclerosis-linked FUS/TLS alters stress granule assembly and dynamics. *Mol Neurodegener*. 2013;8-30:1–18.
 19. Cottrez F, Groux H. Regulation of TGF- β response during T cell activation is modulated by IL-10. *J Immunol* [Internet]. 2001 [cited 2022 Oct 11];167:773–8. Available from: <https://www.jimmunol.org/content/167/2/773>
 20. Hayashi T, Hideshima T, Nguyen AN, Munoz O, Podar K, Hamasaki M, et al. Transforming growth factor β receptor I kinase inhibitor down-regulates cytokine secretion and multiple myeloma cell growth in the bone marrow microenvironment. *Clin Cancer Res* [Internet]. 2004 [cited 2022 Oct 11];10:7540–6. Available from: <https://aacrjournals.org/clincancerres/article/10/22/7540/185424/Transforming-Growth-Factor-Receptor-I-Kinase>
 21. Ma XM, Blenis J. Molecular mechanisms of mTOR-mediated translational control. *Nat Rev Mol Cell Biol*. 2009 [cited 2022 Oct 11];10:307–18. Available from: <https://www.nature.com/articles/nrm2672>
 22. Martin KA, Blenis J. Coordinate regulation of translation by the PI 3-kinase and mTOR pathways. *Adv Cancer Res* [Internet]. 2002 [cited 2022 Oct 11];86:1–39. Available from: <https://pubmed.ncbi.nlm.nih.gov/12374276/>
 23. López-Erauskin J, Tadokoro T, Baughn MW, Myers B, McAlonis-Downes M, Chillon-Marinas C, et al. ALS/FTD-linked mutation in FUS suppresses intra-axonal protein synthesis and drives disease without nuclear loss-of-function of FUS. *Neuron* [Internet]. 2018 [cited 2019 Feb 15];100:816–830.e7. Available from: <https://linkinghub.elsevier.com/retrieve/pii/S0896627318308468>
 24. Aviner R. The science of puromycin: from studies of ribosome function to applications in biotechnology. *Comput Struct Biotechnol J* [Internet]. 2020 [cited 2021 Nov 11];18:1074–83. Available from: <https://pubmed.ncbi.nlm.nih.gov/3229235/>
 25. Birsá N, Ule AM, Garone MG, Tsang B, Mattedi F, Chong PA, FUS-ALS mutants alter FMRP phase separation equilibrium and impair protein translation. *bioRxiv*. 2020;09.14.296038. <https://doi.org/10.1101/2020.09.14.296038>
 26. Kamelgarn M, Chen J, Kuang L, Jin H, Kasarskis EJ, Zhu H. ALS mutations of FUS suppress protein translation and disrupt the regulation of nonsense-mediated decay. *Proc Natl Acad Sci USA* [Internet]. 2018 [cited 2019 Feb 15];115:E11904–13. Available from: <http://www.ncbi.nlm.nih.gov/pubmed/30455313>
 27. Deshpande D, Higelin J, Schoen M, Vomhof T, Boeckers TM, Demestre M, et al. Synaptic FUS localization during motoneuron development and its accumulation in human ALS synapses. *Front Cell Neurosci*. 2019;13:256.
 28. Hong C, Schubert M, Tijhuis AE, Requesens M, Roorda M, van den Brink A, et al. cGAS–STING drives the IL-6-dependent survival of chromosomally unstable cancers. *Nature*. 2022 [cited 2022 Oct 11];607:366–73. Available from: <https://www.nature.com/articles/s41586-022-04847-2>
 29. Korobeynikov VA, Lyashchenko AK, Blanco-Redondo B, Jafar-Nejad P, Shneider NA. Antisense oligonucleotide silencing of FUS expression as a therapeutic approach in amyotrophic lateral sclerosis. *Nat Med*. 2022;28:104–16.
 30. Ishigaki S, Sobue G. Importance of functional loss of FUS in FTL/ALS. *Front Mol Biosci*. 2018;5:44.
 31. Fujii R. TLS facilitates transport of mRNA encoding an Actin-stabilizing protein to dendritic spines. *J Cell Sci* [Internet]. 2005 [cited 2019 Jul 22];118:5755–65. <https://doi.org/10.1242/jcs.02692>
 32. Akbari S, Seyedabadi M, Amiri FT, Naderi M, Shaki F. Sodium arsenite accelerates D-galactose-induced aging in the testis of the rat: evidence for mitochondrial oxidative damage, NF- κ B, JNK, and apoptosis pathways. *Toxicology*. 2022;470:153148.
 33. Vandoorne T, de Bock K, van den Bosch L. Energy metabolism in ALS: an underappreciated opportunity? *Acta Neuropathol* [Internet]. 2018 [cited 2022 Oct 11];135:489–509. Available from: <https://pubmed.ncbi.nlm.nih.gov/29549424/>
 34. Potenza RL, de Simone R, Armida M, Mazziotti V, Pèzzola A, Popoli P, et al. Fingolimod: a disease-modifier drug in a mouse model of amyotrophic lateral sclerosis. *Neurotherapeutics* [Internet]. 2016 [cited 2022 Oct 11];13:918–27. Available from: <https://pubmed.ncbi.nlm.nih.gov/27456702/>
 35. Mirzaei M, Abyadeh M, Turner AJ, Vander WR, Chick JM, Paulo JA, et al. Fingolimod effects on the brain are mediated through biochemical modulation of bioenergetics, autophagy, and neuroinflammatory networks. *Proteomics* [Internet]. 2022 [cited 2022 Oct 11];22:1–14. Available from: <https://europepmc.org/article/med/35866514>
 36. Heitzer C, Kaiser S, Kanagaratnam M, Zendedel A, Hartmann P, Beyer C, et al. Administration of 17 β -estradiol improves motoneuron survival and Down-regulates inflammasome activation in male SOD1(G93A) ALS mice. *Mol Neurobiol* [Internet]. 2016 [cited 2022 Oct 11];54:8429–43. Available from: <https://europepmc.org/article/med/27957680>
 37. Haidet-Phillips AM, Hester ME, Miranda CJ, Meyer K, Braun L, Frakes A, et al. Astrocytes from familial and sporadic ALS patients are toxic to motor neurons. *Nat Biotechnol* [Internet]. 2011 [cited 2022 Oct 11];29:824–8. Available from: <https://pubmed.ncbi.nlm.nih.gov/21832997/>
 38. de Boer AS, Koszka K, Kiskinis E, Suzuki N, Davis-Dusenbery BN, Eggan K. Genetic validation of a therapeutic target in a mouse model of ALS. *Sci Transl Med* [Internet]. 2014 [cited 2022 Oct 11];6:248ra104. Available from: <https://pubmed.ncbi.nlm.nih.gov/25100738/>
 39. Dhandapani KM, Brann DW. Transforming growth factor- β : a neuroprotective factor in cerebral ischemia. *Cell Biochem Biophys*. 2003;39:13–22.
 40. Galbiati M, Crippa V, Rusmini P, Cristofani R, Messi E, Piccolella M, et al. Multiple roles of transforming growth factor beta in amyotrophic lateral sclerosis. *Int J Mol Sci*. 2020;21:1–17.
 41. Prehn JHM, Peruch B, Unsicker K, Kriegstein J. Isoform-specific effects of transforming growth factors- β on degeneration of primary neuronal cultures induced by cytotoxic hypoxia or glutamate. *J Neurochem*. 1993;60:1665–72.
 42. Liu J, Gao L, Zang D. Elevated levels of IFN- γ in CSF and serum of patients with amyotrophic lateral sclerosis. *PLoS One* [Internet].

- 2015 [cited 2022 Oct 11];10:e0136937. Available from: <https://pubmed.ncbi.nlm.nih.gov/26332465/>
43. Rentzos M, Rombos A, Nikolaou C, Zoga M, Zouvelou V, Dimitrakopoulos A, et al. Interleukin-15 and interleukin-12 are elevated in serum and cerebrospinal fluid of patients with amyotrophic lateral sclerosis. *Eur Neurol* [Internet]. 2010 [cited 2022 Oct 11];63:285–90. Available from: <https://pubmed.ncbi.nlm.nih.gov/20407265/>
 44. Jun MH, Ryu HH, Jun YW, Liu T, Li Y, Lim CS, et al. Sequestration of PRMT1 and Ndl-L mRNA into ALS-linked FUS mutant R521C-positive aggregates contributes to neurite degeneration upon oxidative stress. *Sci Rep* [Internet]. 2017 [cited 2022 Oct 11];7:40474–40489. Available from: <https://pubmed.ncbi.nlm.nih.gov/28094300/>
 45. Udagawa T, Fujioka Y, Tanaka M, Honda D, Yokoi S, Riku Y, et al. FUS regulates AMPA receptor function and FTL/ALS-associated behaviour via GluA1 mRNA stabilization. *Nat Commun* [Internet]. 2015 [cited 2022 Oct 11];6:7098–7111. Available from: <https://pubmed.ncbi.nlm.nih.gov/25968143/>
 46. Sephtona CF, Tangc AA, Kulkarnia A, Westa J, Brooksa M, Stubblefielda JJ, et al. Activity-dependent FUS dysregulation disrupts synaptic homeostasis. *Proc Natl Acad Sci USA* [Internet]. 2014 [cited 2022 Oct 11];111:E4769–78. Available from: <https://pubmed.ncbi.nlm.nih.gov/25324524/>
 47. Sévigny M, Julien IB, Venkatasubramani JP, Hui JB, Dutchak PA, Sephton CF. FUS contributes to mTOR-dependent inhibition of translation. *J Biol Chem*. 2020;295:18459–73.
 48. Hashioka S, McGeer E, Miyaoka T, Wake R, Horiguchi J, McGeer P. Interferon- γ -induced neurotoxicity of human astrocytes. *CNS Neurol Disord Drug Targets* [Internet]. 2015 [cited 2022 Oct 11];14:251–6. Available from: <https://pubmed.ncbi.nlm.nih.gov/25687700/>
 49. Beghi E, Chiò A, Inghilleri M, Mazzini L, Micheli A, Mora G, et al. A randomized controlled trial of recombinant interferon beta-1a in ALS. *Neurology* [Internet]. 2000 [cited 2022 Oct 11];54:469–74. Available from: <https://n.neurology.org/content/54/2/469>
 50. Lubina-Dąbrowska N, Stepień A, Sulkowski G, Dąbrowska-Bouta B, Langfort J, Chalimoniuk M. Effects of IFN- β 1a and IFN- β 1b treatment on the expression of cytokines, inducible NOS (NOS type II), and myelin proteins in animal model of multiple sclerosis. *Arch Immunol Ther Exp (Warsz)* [Internet]. 2017 [cited 2022 Oct 11];65:325–38. Available from: <https://europepmc.org/articles/PMC5511332>
 51. Poutiainen E, Hokkanen L, Niemi ML, Färkkilä M. Reversible cognitive decline during high-dose α -interferon treatment. *Pharmacol Biochem Behav*. 1994;47:901–5.
 52. Iivanainen M, Laaksonen R, Niemi M-L, Färkkilä M, Bergström L, Mattson K, et al. Memory and psychomotor impairment following high-dose interferon treatment in amyotrophic lateral sclerosis. *Acta Neurol Scand*. 1985;72:475–80.
 53. Färkkilä M, Iivanainen M, Roine R, Bergström L, Laaksonen R, Niemi M-L, et al. Neurotoxic and other side effects of high-dose interferon in amyotrophic lateral sclerosis. *Acta Neurol Scand*. 1984;70:42–6.
 54. Tang Y, Liu ML, Zang T, Zhang CL. Direct reprogramming rather than iPSC-based reprogramming maintains aging hallmarks in human motor neurons. *Front Mol Neurosci*. 2017;10:359.
 55. Miller JD, Ganat YM, Kishinevsky S, Bowman RL, Liu B, Tu EY, et al. Human iPSC-based modeling of late-onset disease via progerin-induced aging. *Cell Stem Cell*. 2013;13:691–705.
 56. McQuin C, Goodman A, Chernyshev V, Kamensky L, Cimini BA, Karhohs KW, et al. CellProfiler 3.0: next-generation image processing for biology. *PLoS Biol* [Internet]. 2018 [cited 2021 Oct 3];16:e2005970. <https://doi.org/10.1371/journal.pbio.2005970>
 57. Danielson E, de Arce KP, Cimini B, Wamhoff EC, Singh S, Cottrell JR, et al. Molecular diversity of glutamatergic and GABAergic synapses from multiplexed fluorescence imaging. *eNeuro* [Internet]. 2021 [cited 2022 Oct 11];8:1–18. Available from: <https://pmc/articles/PMC7877457/>.

SUPPORTING INFORMATION

Additional supporting information can be found online in the Supporting Information section at the end of this article.

How to cite this article: Assoni AF, Guerrero EN, Wardenaar R, Oliveira D, Bakker PL, Alves LM, et al. IFN γ protects motor neurons from oxidative stress via enhanced global protein synthesis in FUS-associated amyotrophic lateral sclerosis. *Brain Pathology*. 2023. e13206. <https://doi.org/10.1111/bpa.13206>